International Journal of Design & Nature and Ecodynamics
Vol. 21, No. 5, May, 2026, pp. 1339-1351
Journal homepage: http://iieta.org/journals/ijdne

Cinnamaldehyde-Loaded Chitosan Nanoparticles Prepared by Ionic Gelation: In Vitro Activity Against *Candida* Isolates from HIV-Associated Oral Candidiasis

Vita Meylani[1,2], Budi Setiadi Daryono[3], Endah Retnaningrum[4], Satiti Retno Pudjiati[5], Nastiti Wijayanti[6], Tri Wibawa[7*]

[1] Doctoral Program, Faculty of Biology, Universitas Gadjah Mada, Yogyakarta 55281, Indonesia
[2] Department of Biology, Faculty of Mathematics and Natural Sciences, Universitas Papua, Manokwari 98314, Indonesia
[3] Genetics Laboratory, Faculty of Biology, Universitas Gadjah Mada, Yogyakarta 55281, Indonesia
[4] Microbiology Laboratory, Faculty of Biology, Universitas Gadjah Mada, Yogyakarta 55281, Indonesia
[5] Department of Dermatology and Venereology, Faculty of Medicine, Public Health and Nursing, Universitas Gadjah Mada, Yogyakarta 55281, Indonesia
[6] Animal Physiology Laboratory, Faculty of Biology, Universitas Gadjah Mada, Yogyakarta 55281, Indonesia
[7] Department of Microbiology, Faculty of Medicine, Public Health and Nursing, Universitas Gadjah Mada, Yogyakarta 55281, Indonesia

Corresponding Author Email: twibawa@ugm.ac.id

https://doi.org/10.18280/ijdne.210511

Received: 3 March 2026
Revised: 15 May 2026
Accepted: 22 May 2026
Available online: 31 May 2026

Keywords:
nanoencapsulation, cinnamaldehyde, chitosan, Candida albicans, Human Immunodeficiency Virus

ABSTRACT

Oral candidiasis is a common opportunistic infection in Human Immunodeficiency Virus (HIV) patients, significantly affecting their quality of life. This study examined the in vitro efficacy of nanoencapsulated cinnamaldehyde-chitosan as an innovative treatment for oral candidiasis in HIV patients in Yogyakarta, Indonesia. Cinnamaldehyde, a natural antifungal agent, was encapsulated in chitosan nanoparticles to enhance its bioavailability and activity. This study used a combination of in vitro antifungal assays to evaluate the efficacy of the nanoencapsulated formulation against *Candida* species isolated from HIV-infected patients. The cinnamaldehyde-loaded chitosan nanoparticles demonstrated promising in vitro antifungal activity against *C. albicans* isolates associated with HIV-related oral candidiasis, with minimum inhibitory concentration (MIC) values ranging from 0.195% to 1.56%. The formulation demonstrated improved antifungal performance compared with chitosan nanoparticles (6.25%), along with enhanced stability and controlled-release properties. In addition, the nanoformulation exhibited favorable stability and sustained release characteristics, supporting its potential for further antifungal formulation development. Cinnamaldehyde-loaded chitosan nanoparticles with a size of 261.99 ± 21.06 nm, with a polydispersity index (PdI) of 0.252 and a zeta potential of +19.34 ± 0.71 mV, showed a relatively uniform and stable distribution and little aggregation. Fourier Transform Infrared Spectroscopy (FTIR) analysis showed the presence of organic molecules and aromatic amine groups, and UV-Vis spectrophotometer measurements at a wavelength of 225 nm with an absorbance of 2.882 indicated a high and stable concentration of cinnamaldehyde chromophore in the nanoencapsulation. Transmission Electron Microscopy (TEM) analysis showed spherical particles at the nanoscale morphology with a smooth and irregular surface; whereas Scanning Electron Microscopy (SEM) mainly showed dried aggregates surface morphology, demonstrating the typical core-shell architecture of the nanoencapsulation system. This study underscores the potential use of nanotechnology as a stable, prolonged-release antifungal formulation for oral candidiasis, which presents a promising approach to improve health outcomes for HIV patients.

1. INTRODUCTION

Oral candidiasis is one of the most common opportunistic fungal infections in individuals with Human Immunodeficiency Virus (HIV) / Acquired Immune Deficiency Syndrome (AIDS), with prevalence rates ranging from 7.6% to 75.3% depending on the population studied [1, 2]. Its occurrence is strongly associated with immunosuppression and disease progression. The management of oral candidiasis in HIV-positive patients has become increasingly challenging because of the growing resistance of *Candida* spp. to antifungal agents, particularly azoles such as fluconazole [2, 3]. Resistance rates of up to 39.3% have been reported among *Candida* isolates from HIV patients, affecting both *Candida albicans* and non-albicans *Candida* species [2, 3]. In addition, prolonged systemic

antifungal therapy may cause adverse effects and drug interactions, limiting treatment effectiveness [4].

Cinnamaldehyde, the major bioactive compound of cinnamon essential oil, has demonstrated broad antifungal activity against pathogenic fungi, including *Candida* spp. Its antifungal mechanisms involve disruption of fungal cell membranes, inhibition of essential enzymes, and induction of oxidative stress [5-8]. However, the clinical application of cinnamaldehyde is restricted by its poor water solubility, high volatility, and instability under environmental conditions such as light and oxidation [9, 10]. These limitations may reduce bioavailability and therapeutic efficacy.

Nanoencapsulation strategies using chitosan have been developed to improve the stability and delivery of cinnamaldehyde [6, 9, 11]. Chitosan nanoparticles exhibit high encapsulation efficiency and controlled-release properties, which enhance cinnamaldehyde stability and prolong its antifungal activity [12-16]. Encapsulated *Cinnamomum verum* essential oil has shown stronger antifungal efficacy against *C. albicans* compared with its non-encapsulated form, with reported minimum inhibitory concentration (MIC) values of 125 µg/mL [13]. In addition, chitosan-based nanoformulations possess favorable biocompatibility and mucoadhesive properties, making them suitable for oral drug delivery applications [15, 17, 18]. Previous studies also demonstrated that cinnamaldehyde-loaded chitosan nanoparticles exhibited lower cytotoxicity than non-encapsulated essential oils while maintaining effective antifungal activity [3].

Besides their antifungal potential, chitosan–cinnamaldehyde nanoformulations have shown promising antibacterial, antioxidant, and biomedical properties, including applications in drug delivery systems and tissue engineering [16, 19-22]. These findings indicate that nanoencapsulation may represent a promising strategy to enhance the therapeutic potential of cinnamaldehyde against oral candidiasis associated with HIV infection.

2. MATERIAL AND METHODS

2.1 Fabrication of chitosan nanoparticles

The chitosan nanoparticle formulation was prepared using the ionic gelation process with minor changes [6]. Chitosan nanoparticles were synthesised by dissolving 0.2% (w/v) chitosan in 1% acetic acid and subsequently homogenising with a stirrer for 48 hours until fully dissolved. A 0.2% phosphate (TPP) solution was administered dropwise at a rate of 0.2 mL/min using a syringe pump into the chitosan solution. The solution's pH was assessed and modified to pH 5. The chitosan and TPP combination was sonicated at 80% amplitude for 3 hours, with intervals of 30 minutes, to create a nanosuspension. The resultant nanosuspension was thereafter held at 4 ℃ for cooling and allowed to rest for approximately 7 days prior to further testing.

2.2 Fabrication of cinnamaldehyde-chitosan nanoencapsulation

The procedure for synthesizing cinnamaldehyde-chitosan nanoencapsulation is based on the methodology employed by research [16] with several modifications. A 0.1% Tween 80 solution, followed by homogenization at room temperature at 1000 rpm for 3 hours. Next, the chitosan solution, formulated as a nanosuspension, is subsequently dissolved in the 0.1% Tween 80 solution and heated to 50 ℃. A specified quantity of cinnamaldehyde is incorporated into the solution at a weight ratio of 1:0.40 (w/w) while maintaining continuous stirring and emulsified at 1200 rpm for 20 minutes at ambient temperature. a 0.2% TPP solution was administered dropwise at a rate of 2 mL while stirring continuously at 700 rpm for 40 minutes; subsequently, the nanoparticles were harvested by centrifugation of the resultant solution at 10,000 rpm for 40 minutes at 4 ℃, followed by multiple washes with mQ water to eliminate any unencapsulated cinnamaldehyde. The nanoencapsulated slurry was subsequently kept at 4 ℃ for additional testing.

The nanoencapsulation process was optimized by controlling several formulation parameters, including ultrasonic treatment intensity and duration, stirring conditions, and pH adjustment during chitosan crosslinking. The pH of the formulation was adjusted to 5.0, while ultrasonication was performed at 80% for 3 hours with 30 minutes per cycle to obtain stable nanoparticles. Batch uniformity was evaluated by comparing particle size, polydispersity index (PdI), and zeta potential among independently prepared batches, which demonstrated consistent physicochemical characteristics. No specific vehicle control containing formulation excipients alone (e.g., Tween or heptane) was included in the present study.

2.3 Characterization of cinnamaldehyde-chitosan nanoencapsulation

The characterization of chitosan nanoparticles encompasses various characteristics [23], specifically:

2.3.1 Particle size analyzer, polydispersity index, and zeta potential test

The particle size analyzer (PSA), PdI, and zeta potential assessments of cinnamaldehyde-chitosan nanoencapsulation (1 g/L in deionized water) were conducted at 25 ℃, with ten repeats. The PSA and PdI measurements employed the Dynamic Light Scattering (DLS) technique, which measures the intensity of light scattered by the Brownian motion of particles in a liquid, subsequently processing the signal to swiftly and accurately determine particle distribution and size [24, 25]. This test is conducted to ascertain particle size and zeta potential.

Particle size distribution analysis was performed using DLS, and all particle diameter measurements are reported in nanometers (nm). The original instrument output data were re-evaluated to verify measurement accuracy and unit consistency.

2.3.2 Fourier Transform Infrared Spectroscopy analysis

The chitosan nanoparticles were individually combined with potassium bromide (KBr), ground, and compressed to create slices. Spectra were acquired in the infrared range of 400–4000 cm^{-1} utilizing Fourier Transform Infrared Spectroscopy (FTIR), with 32 scans and a resolution of 4 cm^{-1} [25].

2.3.3 Transmission Electron Microscopy analysis

For Transmission Electron Microscopy (TEM) observation, dilute the chitosan nanoparticles with ultrapure water, then deposit a drop of the solution onto a standard copper grid coated with a holey carbon (C) layer and allow it to dry at room

temperature (37.5 ℃). Subsequently, visualize using TEM at an accelerating voltage of 40–120 kV. This test is conducted to examine the microstructure of the cinnamaldehyde-chitosan nanoencapsulations [24, 25].

2.3.4 UV/VIS spectroscopy analysis

Nanoencapsulated cinnamaldehyde-chitosan and pure conjugated linoleic acid (CLA) were diluted 1:10000 with heptane and placed into a 1 cm quartz cell. Absorption was quantified within the range of 190 to 300 nm. Pure heptane was utilized as a control [25].

2.4 Scanning Electron Microscopy – Energy Dispersive X-ray analysis

Dried nanoencapsulations are created on a grid or Scanning Electron Microscopy (SEM) holder and subsequently coated with gold for SEM-Energy Dispersive X-ray Spectroscopy (EDX) observations. High magnification images are utilized to examine the distribution and dimensions of the particles, typically ranging from 190 to 300 nm. Following the acquisition of the SEM picture, an EDX study, a technique based on X-ray spectroscopy, is conducted. This test characterizes the surface shape and elemental content of the nanoencapsulation.

2.5 Antifungal susceptibility testing

2.5.1 Identification of *C. albicans*

A total of eight clinical *C. albicans* isolates were obtained from oral swab specimens collected from HIV-positive patients clinically diagnosed with oral candidiasis at Sardjito Hospital. Samples were collected from lesions located on the oral mucosal surfaces, including the tongue, buccal mucosa, and palate. Inclusion criteria consisted of HIV-positive patients presenting clinical signs of oral candidiasis and yielding positive fungal cultures. Patients who had received systemic antifungal treatment with fluconazole before sampling were excluded for at least 3 months. Initial identification was performed based on colony morphology and microscopic examination. Species confirmation was conducted using CHROMagar *Candida* identification methods, and only confirmed *C. albicans* isolates were included in the antifungal susceptibility testing. Species confirmation was performed using CHROMagar *Candida* based on characteristic colony coloration.

In addition to the clinical *C. albicans* isolates, the reference strain *C. albicans* ATCC 14053 was included as a quality control strain during antifungal susceptibility testing. The reference strain was used to provide a standardized comparison and to ensure the reliability and consistency of the broth microdilution assay conditions.

2.5.2 Microdilution method to determine the minimum inhibitory concentration of cinnamaldehyde-chitosan nanoencapsulation as an antifungal

Antifungal activity testing was performed using a broth microdilution method adapted from the Clinical and Laboratory Standards Institute (CLSI) M27 guideline for yeasts. *Candida* isolates were subcultured on Sabouraud Dextrose Agar (SDA) and incubated at 35 ℃ for 24 hours. Several colonies were suspended in sterile 0.85% saline solution and adjusted spectrophotometrically to match a 0.5 McFarland standard turbidity, corresponding to approximately 1.5×10^8 CFU/mL. The suspension was subsequently diluted 1:1000 in Roswell Park Memorial Institute (RPMI)-1640 medium buffered with 0.165 M 3-(N-morpholino) propanesulfonic acid (MOPS) (pH 7.0) to obtain a final inoculum concentration of approximately 0.5–2.5 × 10^5 CFU/mL in each well [25].

Serial two-fold dilutions of cinnamaldehyde-loaded chitosan nanoparticles were prepared in RPMI-1640 medium at concentrations ranging from 0.195% to 1.56% (v/v). Each dilution (100 µL) was mixed with 100 µL of standardized fungal inoculum in sterile 96-well microplates. Growth and sterility controls were included, and fluconazole was used as a positive antifungal control where applicable. After incubation at 35 ℃ for 24–48 h, the MIC was determined as the lowest concentration showing complete visible inhibition of fungal growth compared with the untreated growth control. All assays were performed in triplicate to ensure reproducibility.

The MIC values reported in this study represent the percentage concentration (v/v) of cinnamaldehyde-loaded chitosan nanoparticle suspension relative to the total assay volume. Serial two-fold dilutions were prepared from a stock suspension containing 28 mg/mL cinnamaldehyde to obtain final concentrations ranging from 54.6–1750 µg/mL, corresponding to approximately 6.25% to 0.195% (v/v) cinnamaldehyde equivalent concentrations. Free cinnamaldehyde and blank chitosan nanoparticles were evaluated under identical conditions using the same concentration range, with blank chitosan nanoparticles serving as the nanoparticle control. MIC values were determined using a broth microdilution method adapted from CLSI antifungal susceptibility testing guidelines.

All antifungal susceptibility assays were performed in triplicate under identical experimental conditions to ensure reproducibility and reliability of MIC determination. A reference strain, *C. albicans* ATCC 14053, was included as a control for assay standardization. Consistent MIC values were obtained across independent replicate experiments, and the data were analyzed descriptively to evaluate antifungal activity patterns among the tested formulations.

Several controls were incorporated into the broth microdilution assay to ensure the reliability of the antifungal susceptibility results. Sterility control wells containing only RPMI-1640 medium were included to confirm the absence of contamination, while growth control wells containing fungal inoculum without treatment were used to verify normal fungal growth. However, vehicle controls and standard antifungal drug comparisons were not comprehensively evaluated in the present study and are recognized as important limitations. Future studies should incorporate these controls to better distinguish the specific antifungal contribution of each formulation component and to allow standardized comparison with clinically used antifungal agents.

2.5.3 Examination of morphological structural damage in *C. albicans* isolates post-nanoencapsulation employing Scanning Electron Microscopy

The morphology of freeze-dried nanocapsules was analyzed using an SEM to investigate the powder surface structure. Samples were affixed to adhesive tape on specimen pieces, and the particles were coated with gold-palladium before examination.

3. RESULT AND DISCUSSIONS

3.1 Size, homogeneity, and zeta potential of cinnamaldehyde-chitosan nanoencapsulation

Table 1. The results of the particle size analyzer (PSA), polydispersity index (PdI), and zeta potential measurement

Sample	Size (nm)	Polidispersity Index (PdI)	Zeta Potential (mV)
Trial 1	244.2	0.242	+19.1 ± 1.33
Trial 2	287.2	0.257	+19.8 ± 1.82
Trial 3	255.9	0.231	+19.3 ± 1.61
Trial 4	232.2	0.279	+18.5 ± 1.35
Trial 5	247.6	0.235	+20.7 ± 1.68
Trial 6	276.1	0.273	+20.0 ± 1.64
Trial 7	300.8	0.247	+18.7 ± 1.70
Trial 8	261.5	0.269	+18.8 ± 1.71
Trial 9	248.3	0.241	+18.7 ± 1.87
Trial 10	266.1	0.242	+19.8 ± 1.52
Mean ± SD	261.99 ± 21.06 nm	0.252 ± 0.017	+19.34 ± 0.71 mV

Table 1 indicates that the mean nanoparticle size of 262 nm falls inside the fine particle classification. In certain situations, particularly in pharmaceutical or nanotechnology applications, diameters ranging from 200 to 400 nm remain pertinent for nanoparticle applications due to their comparable qualities and behavior to core nanoparticles [26]. The mean zeta potential measurement of chitosan-cinnamaldehyde nanoencapsulation is +19.34 ± 0.71 mV, signifying that the nanoparticles possess a positive surface charge and exhibit moderate colloidal stability [25]. A high zeta potential value, either positive or negative (often above +30 mV or falling below -30 mV), signifies effective dispersant stability resulting from robust repulsive forces that inhibit particle aggregation [27, 28].

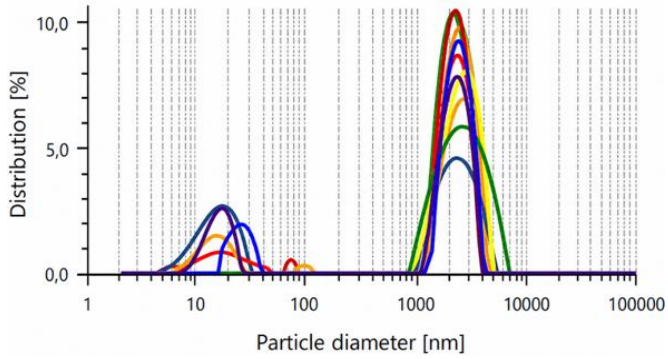

Figure 1. Dynamic Light Scattering (DLS) analysis of cinnamaldehyde-loaded chitosan nanoparticles showing particle size distribution in nanometers (nm)

The nanoparticles (Figure 1) showed an average particle size of 261.99 nm, consistent with the expected nanoscale range for chitosan-based nanoparticle systems. The presence of two distinct size populations can have several meanings of bimodal distributions (with a primary peak around approximately 2,000 nm or 2 µm and a secondary peak at 20 nm), which are often a signature of aggregation processes, formulation design, measurement artifacts, and colloid stability theory. Bimodal distributions often signal aggregation, where small primary particles clump into larger aggregates over time. Experimental studies in colloidal and sediment systems show that initially unimodal distributions can evolve into bimodal ones as aggregation or flocculation progresses, with the large-size peak growing as aggregates form [26].

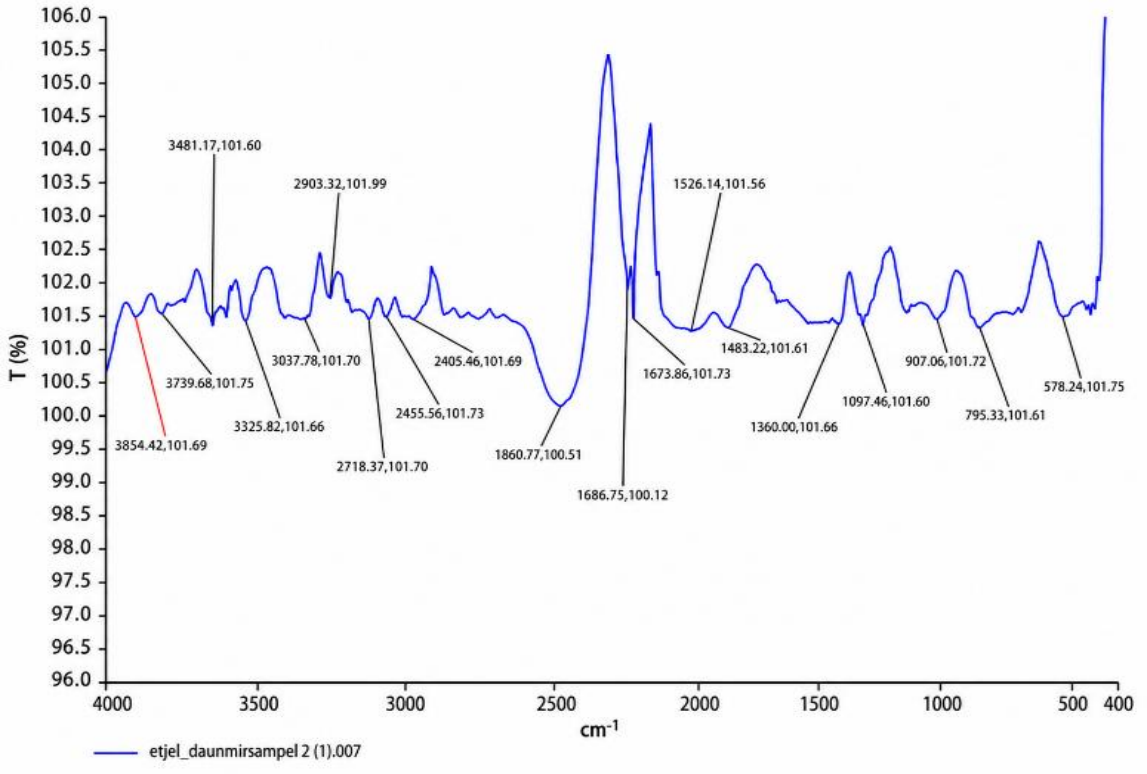

Figure 2. The Fourier Transform Infrared Spectroscopy (FTIR) spectrum of the nanoparticle samples shows absorption bands at various wavenumbers (cm^{-1}), indicating the presence of certain functional groups

3.2 Molecular structure and chemical composition of cinnamaldehyde-chitosan nanoencapsulation

Figure 2 shows that interpreting FTIR spectra involves associating specific wavenumber regions and peak characteristics with molecular vibrations and functional groups. Broad absorption around ~3420–3850 cm^{-1} indicates O–H (hydroxyl) or N–H (amine) stretching vibration, which comes from chitosan and bound water, which often appears after encapsulation. Peaks near ~2900 cm^{-1} represent C–H stretching, while the sharp band around ~1650 cm^{-1} suggests C=O stretching (carbonyl groups), typical of amide bonds from Chitosan or encapsulation interactions. Bands in the ~1000–1100 cm^{-1} region indicate C–O (glycosidic structure of chitosan) or C–N (secondary amine groups) stretching vibrations, confirming the presence of functional modifications in the nanoparticle structure [29, 30]. When compared to pure chitosan, changes in intensity or shifts in wave numbers (red/blue shift) indicate successful chemical interactions or nanoparticle formation. In addition, the strong amide I & II bond structure (1686 and 1526 cm^{-1}) indicates the possibility of chemical interactions or complexation between chitosan and active ingredients or crosslinking agents (such as TPP) [31]. Furthermore, the absorption bond structure in the 1000–1100 cm^{-1} area indicates a polysaccharide framework, which is important to identify the presence of the chitosan structure [32].

3.3 Morphological structure of cinnamaldehyde-chitosan nanoencapsulation

Figure 3(a) indicates the particle has a diameter of approximately 170-190 nm. The uniform spherical morphology suggests colloidal synthesis or controlled deposition [33]. TEM observations revealed nanoparticles with spherical morphology and sizes more directly measurable at the nanometer scale [34, 35]. The particle sizes of chitosan cinnamaldehyde nanoencapsulation reported using TEM are typically in the range of tens to approximately 200 nanometers [36, 37]. Chitosan cinnamaldehyde nanoparticles with average diameters between 65 and 208 nm were reported, indicating good sphericity and a core-shell structure typical for nanoencapsulation systems [38]. Figure 3(b) indicates the particle is approximately 140–160 nm in diameter. There's also a smaller bright feature to the left, likely a smaller nanoparticle or crystallite [39]. The dark rim suggests the presence of a higher atomic number shell, possibly a metallic layer [36, 37]. The lighter core could be an organic or polymer material, such as a functionalized core or stabilizer matrix [34, 35]. This structure is typical of core-shell nanoparticles, encapsulated drug delivery systems, and functionalized gold nanospheres [36, 37].

3.4 Optical properties of cinnamaldehyde-chitosan nanoencapsulation

Figure 4 shows that the absorbance peak of Chitosan Nanoencapsulation is at a wavelength of 205 nm with an absorbance of 2.783. After adding Cinnamaldehyde, the absorbance peak is at a wavelength of 225 nm with an absorbance of 2.882. This maximum absorption reflects the electron transition that occurs due to changes in the chemical structure of the chromophore properties in cinnamaldehyde and the formation of stable nanoparticles. The shift in the absorbance peak and its intensity is an indicator of the success of the synthesis of these nanoparticles. In the UV-Vis curve, after the maximum peak, the absorption intensity decreases gradually, indicating a typical spectrum of nanoparticles [40]. At a wavelength of 225 nm, including the UV-C region, it usually shows the π-π * electron transition of the carbonyl group or aromatic group.

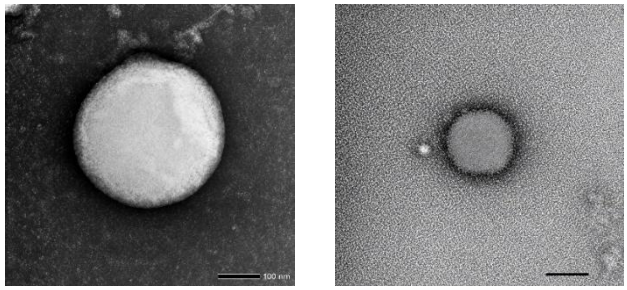

(a) (b)

Figure 3. The high-resolution Transmission Electron Microscopy (TEM) image showing (a) a single spherical nanoparticle bar, at 100 nm, and (b) a core-shell type nanoparticle or a coated nanoparticle bar, at 200 nm

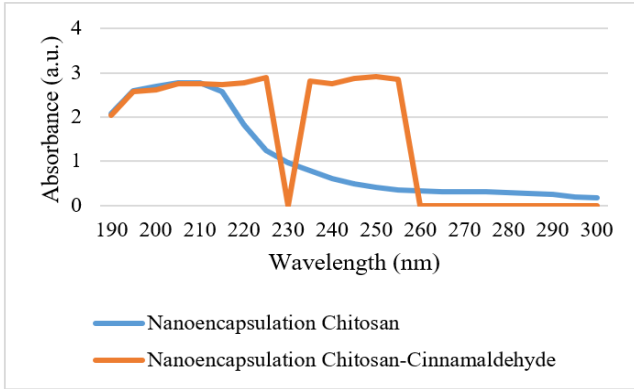

Figure 4. UV-Vis absorbance spectra for two samples: pure chitosan nanoencapsulation (blue line) and chitosan-cinnamaldehyde nanoencapsulation (orange line) in the wavelength range 190–300 nm

3.5 Material characterization of cinnamaldehyde-chitosan nanoencapsulation

Figure 5 shows that chitosan-cinnamaldehyde nanoencapsulation has a scale bar of 50 µm (micrometers), indicating relatively large structures. The sample contains irregular, angular, and flaky particles, consistent with a crushed or fragmented material, possibly a mineral, polymer composite, or bio-based material [41, 42]. The particles vary in size and shape, indicating heterogeneous morphology. Spc_008 (blue square) targets a flat, elongated particle — likely selected for elemental composition analysis by EDX. Meanwhile, Spc_007 (red square) covers a rougher, more aggregated area — possibly chosen for compositional comparison. Figure 5(a) shows that the particles vary in size and shape, indicating heterogeneous morphology. Spc_008 (blue square) targets a flat, elongated particle — likely selected for elemental composition analysis by EDX. Meanwhile, Spc_007 (red square) covers a rougher, more aggregated area — possibly chosen for compositional comparison.

Sample Surface of Figure 5(b) contains irregularly shaped, fractured, and layered particles, likely from a crushed or

processed solid material. These particles are uneven and appear to have porous and flaky textures, suggesting a natural material (e.g., biomass or mineral) or a composite or aggregate structure. Spc_009 is marked with a green square in the lower central region. Likely a selected region for EDX analysis to determine local elemental composition. Positioned over a zone with finer texture and possibly differing morphology from surrounding bulk particles.

Figure 5 has a scale bar of 50 µm, giving context to the size of particles — many are in the 10–100 µm range.

Figure 6 is an EDX spectrum, which detected element C Kα (~0.27 keV) with a strong peak indicating the presence of C. O Kα (~0.53 keV) with a smaller but clear peak, indicating oxygen (O). And gold (Au) peaks with Au M-series (Mα, Mb, Mz, Mr) with peaks in the range of ~2 to 3 keV. Au L-series (Lα, Lβ, Lγ, etc.) with peaks spread out from ~9.7 to ~14 keV (e.g., AuLα, AuLb1, AuLb2, AuLr). And the multiple peaks suggest a significant presence of gold (Au) in the sample.

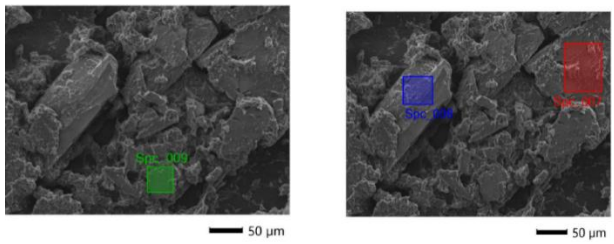

(a) (b)

Figure 5. The Scanning Electron Microscopy (SEM) micrograph, showing a high-resolution surface morphology of a solid sample (a) Spc_009 (green square) is a natural material bi-based composite aggregate structure, and (b) polymer composite includes Spc_008 (blue square), a flat, elongated particle, and Spc_007 (red square) covers a rougher, more aggregated area

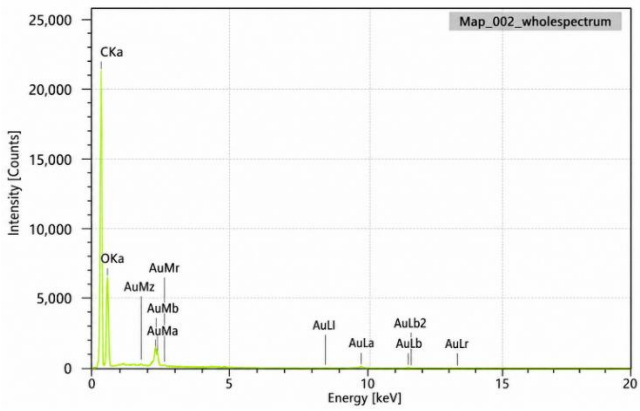

Figure 6. The Energy Dispersive X-ray Spectroscopy (EDX) spectrum for the whole spectrum

Figure 7 shows that the background image is a grayscale SEM image of a rough, fragmented surface with various particle sizes and textures. EDX analysis of the cinnamaldehyde-loaded chitosan nanoparticles primarily showed dominant C and O signals, which are consistent with the organic polymeric composition of chitosan and cinnamaldehyde-based materials. Gold (Au) peaks were also detected; however, these signals originated from the gold sputter-coating applied during SEM sample preparation and do not represent an inherent component of the nanoparticles.

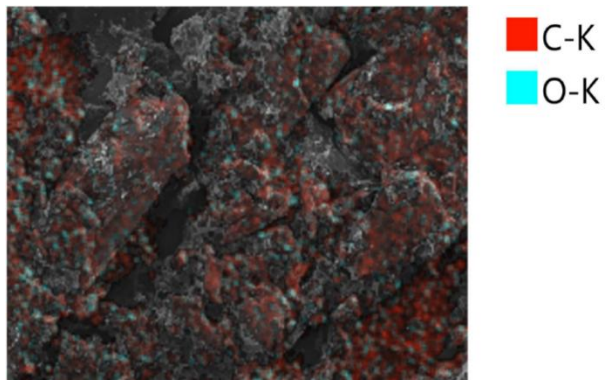

Figure 7. SEM-EDX spectrum of cinnamaldehyde-loaded chitosan nanoparticles

Notes: Gold (Au) peaks originate from sputter coating during SEM preparation. SEM: Scanning Electron Microscopy, EDX: Energy Dispersive X-ray Spectroscopy.

3.6 Antifungal test of cinnamaldehyde-chitosan nanoencapsulation

Antifungal nanoencapsulation testing using the Microdilution method is usually carried out to determine the smallest concentration of nanoencapsulation that is able to inhibit the growth of *C. albicans*. Antifungal tests have been carried out on 8 *Candida* isolates isolated from HIV patients. The results of the antifungal test showed that 7 *C. albicans* isolates originating from HIV patients had different MIC values. Consistent MIC values were observed across triplicate experiments, indicating reproducibility of the antifungal susceptibility results obtained for the tested formulations. The MIC values of cinnamaldehyde-loaded chitosan nanoparticles ranged from 54.6–3500 µg/mL, corresponding to approximately 0.195% to 1.56% (v/v nanoparticle suspension) cinnamaldehyde equivalent concentration (Figure 8). Isolate DV 1, DV2 have an MIC value of 218 µg/mL cinnamaldehyde equivalent to 0.78% (v/v), DV 3 had an MIC value of 54.6 µg/mL cinnamaldehyde equivalent to 0.195% (v/v), DV 4, DV 6, DV 7, and DV 8 have an MIC value of 437 µg/mL cinnamaldehyde equivalent to 1.56% (v/v). DV5 was not detected with an MIC value because the particles aggregate in aqueous solutions, thereby reducing the surface area available for cellular uptake and interaction with the *Candida albicans* cell wall or membrane.

The MIC values for DV 1-8 isolates varied between 0.195% and 1.56%. It signifies a fluctuation in the fungus's susceptibility to the used nanoparticles or active chemicals. Lower values, such as 0.19% for DV 3 isolates, signify greater inhibitory efficacy compared to higher MIC values, such as 1.56% for DV 4, 6, 7, and 8 isolates. The MIC of 0.19% for DV 3 isolates demonstrates the formulation's efficacy at low doses against these isolates, but other isolates necessitate greater values (up to 1.56%). The encapsulation safeguards cinnamaldehyde from degradation, extends its release, and markedly enhances its bioactivity relative to free cinnamaldehyde [43]. The antifungal activity observed in this study was compared with that of chitosan nanoparticles at a concentration of 6.25%. However, direct comparative evaluation against free cinnamaldehyde, vehicle-only formulations, and standard antifungal agents, including fluconazole, nystatin, or micafungin, was not performed in the present study. Therefore, the observed antifungal activity should be interpreted within the limitations of the current experimental design.

Figure 8. Results of the microdilution method to determine the minimum inhibitory concentration (MIC) of cinnamaldehyde-chitosan nanoencapsulation as an antifungal

The MIC values of cinnamaldehyde-loaded chitosan nanoparticles ranged from 0.195% to 1.56% (54.6–437 µg/mL cinnamaldehyde equivalent), depending on the *Candida* isolate tested. Free cinnamaldehyde also demonstrated antifungal activity within the tested concentration range, whereas blank chitosan nanoparticles showed weaker inhibitory activity, with the best MIC observed at 6.25% (v/v). These findings indicate that nanoencapsulation improved the antifungal performance and stability of cinnamaldehyde compared with blank nanoparticles alone.

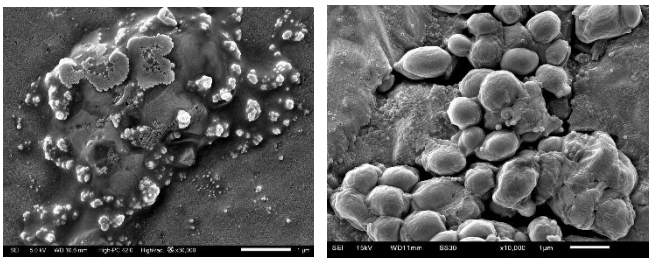

(a) (b)

Figure 9. A Scanning Electron Microscopy (SEM) micrograph, showing a high-resolution surface morphology of a solid sample: (a) before nano-encapsulation, (b) after nano-encapsulation

3.7 Morphological structural damage in *C. albicans* isolates post-nanoencapsulation

The results of morphological structural damage in *Candida albicans* isolates post-nanoencapsulation assessed by SEM provide critical insights into the physical effects of nanoformulations on fungal cells. SEM allows for high-resolution visualization of *C. albicans* cells, revealing changes in cell shape, surface texture, and integrity after treatment. Typically, nanoencapsulation induces notable structural disruptions such as cell wall deformation, surface roughening, shrinkage, and collapse, which reflect the antifungal impact of the encapsulated agent. These morphological alterations often correlate with inhibited fungal growth and biofilm formation, suggesting that nanoencapsulation enhances the delivery and efficacy of antifungal compounds by directly compromising cell membrane and wall stability. Overall, SEM analysis of *C. albicans* post-nanoencapsulation offers valuable evidence of the mechanism of action and potential of nanotechnology-based antifungal strategies.

Figure 9 shows Ne-CC has a scale bar of 1-5 µm (micrometers), indicating relatively spherical or nearly spherical/spherical nanoparticle aggregates or clusters with porous and uneven surfaces that show typical properties for chitosan polymer-based nanoparticles with functional active compounds such as cinnamaldehyde.

3.8 Discussion

This study analyzes the potential of cinnamaldehyde-chitosan nanoencapsulation as an antifungal for *C. albicans* in patients with HIV-oral candidiasis. The average PdI value of 0.252 for chitosan cinnamaldehyde nanoparticles signifies a relatively uniform particle size distribution and a commendable degree of homogeneity [44, 45]. The PdI value indicates the uniformity or diversity of particle sizes within the solution. PdI values between 0.1 and 0.3 are deemed acceptable in pharmaceutical and nanotechnology applications, signifying reasonably homogeneous particle size [16, 19]. Nanoencapsulation of cinnamaldehyde in chitosan-based systems typically yields spherical nanoparticles with diameters ranging from 10 to 370 nm, encapsulation efficiencies between 7% and 91%, and positive zeta potentials, indicating high stability [16, 19]. Consequently, nanoparticles with a PdI of 0.252 demonstrate a favorable size distribution and possess sufficient stability for many research and industrial applications. Particle aggregation or clumping may occur if other parameters, such as medium conditions, fluctuate [46]. Despite the zeta potential value remaining beneath the +30 mV threshold, the nanoparticles exhibit a positive repulsive force; yet, it is insufficient to guarantee optimal stability. Consequently, the dispersion may exhibit considerable stability; nonetheless, the possibility for agglomeration is greater than it would be with a higher zeta value [47]. The stability of the zeta potential can be enhanced by optimizing the nanoparticle formulation through pH adjustment or the incorporation of a stabilizer [26]. Accurate reporting of nanoparticle size units is essential because particle diameter directly influences surface area, stability, drug release behavior, mucoadhesion, and biological interaction. The corrected DLS unit presentation confirms that the formulated particles are within the nanometer scale appropriate for nanoparticle-based drug delivery systems.

Bimodal distributions may be intentionally engineered by mixing small and large particles to optimize properties such as packing density, mechanical strength, or controlled release. In additive manufacturing and ceramics, such mixtures improve density and performance compared to unimodal systems [48]. Occasionally, bimodal distributions can result from measurement artifacts, such as dust or contaminants, introducing a spurious large-size peak. However, if the large-size peak is dominant and reproducible, it is more likely to be intentional or intrinsic to the system rather than an artifact. If both size populations remain stable over time, the system may be kinetically stable but thermodynamically metastable. This means that while aggregates are prevented from further growth by steric or electrostatic repulsion, the system is not in its lowest-energy state [29, 49]. From a physicochemical perspective, a narrow peak width in the main mode (0.1–0.3 µm) indicates low polydispersity, which is beneficial for reproducible behavior in flow systems and biological environments. Low polydispersity ensures consistent particle interactions and predictable system performance, as seen in

studies of both natural and engineered colloidal systems [49]. A small secondary peak at the nanometer scale may represent unincorporated drug molecules, residual surfactant micelles, or intentionally free nanoparticles. In nanoparticle formulations, such secondary populations are often observed and can be attributed to incomplete incorporation or the presence of stabilizing agents.

The results of FTIR and UV-Visible measurements enable the identification of key chemical bonds, assess material purity, and monitor structural changes, making it an essential tool in fields ranging from materials science to biomedical research [29, 49]. The FTIR spectrum shows the presence of the main functional groups of chitosan and a strong indication of chemical interactions between chitosan and other components in the nanoparticle system. This confirms that the nanoencapsulation process or the formation of chitosan-based nanoparticles was successful.

The morphology of nanoencapsulation show nanoencapsulation is able to make easy its optimal potential in drug delivery to the target. The results of TEM analysis of cinnamaldehyde-chitosan nanoencapsulation reveal successful formation of nanoparticles with distinct morphological characteristics [6, 50]. The TEM images typically show well-dispersed, spherical nanoparticles, verifying the successful encapsulation of cinnamaldehyde within the chitosan matrix [50]. The particle size observed through TEM usually ranges from around 65 nm to 300 nm, depending on the preparation method and cinnamaldehyde loading [16]. Such nanoencapsulation leads to a reduction in zeta potential compared to pure chitosan nanoparticles, indicating surface interaction between chitosan and cinnamaldehyde [6, 50]. The range of 200-300 nm is common for aldehyde-aromatic compounds and polyphenols, which indicates the presence of chemical interactions and the possibility of good stability of the encapsulated nanoparticles. Thus, the results of the UV-Vis spectrum with an absorbance peak of 2.882 at 225 nm indicate that the nanoencapsulation of cinnamaldehyde chitosan was successful, and the chromophore effect of cinnamaldehyde was detected strongly at that wavelength.

The composition of nanoencapsulation enhances the stability of *C. albicans* antifungal activity. The strong C and O peaks suggest the presence of organic or oxide materials. The numerous gold peaks imply that the sample contains a substantial amount of gold, either as a coating or part of the material. The shape and intensity of the peaks are typical of qualitative EDX analysis, showing what elements are present and giving a rough idea of their relative abundance. C (red) is widely distributed across the surface, suggesting an organic or C-rich matrix or coating. O (cyan) appears in localized patches, indicating the presence of oxides or O-containing compounds in specific regions. The co-distribution in some areas (where red and cyan overlap) may suggest compounds containing both elements, such as organic materials, carbonates, or oxides. This type of image is typically used to understand the elemental composition and spatial relationships of materials on a microstructural level, such as in geological samples, catalysts, or composite materials.

The EDX analysis was used only as a complementary characterization method to support SEM observations. Since polymeric nanoparticles are predominantly composed of organic elements such as C and O, the obtained spectra mainly reflected these elemental signals. The detected gold (Au) peaks were attributed to the sputter-coating process required for SEM imaging and were not interpreted as part of the nanoparticle formulation. Gold coating is commonly applied to improve conductivity and image quality during SEM examination of non-conductive polymeric materials, and Au-related peaks are therefore frequently observed in EDX spectra of coated samples [51, 52]. Furthermore, EDX analysis of chitosan-based and other organic nanoparticles generally provides limited elemental information due to the predominance of light elements such as C, O, and nitrogen in the formulation matrix [53, 54]. Therefore, no further compositional interpretation of Au signals was made.

The present study utilized eight clinical *C. albicans* isolates obtained from HIV-associated oral candidiasis cases. However, detailed characterization of the isolates, including molecular species confirmation, antifungal susceptibility background, resistance mechanisms, and patient antifungal exposure history, was not comprehensively available. Such factors may substantially influence antifungal responsiveness and could partly explain the variability observed in MIC values among isolates. Prior azole exposure, recurrent infection status, biofilm-forming ability, and strain-specific virulence characteristics are known to contribute to differences in antifungal susceptibility among *Candida* isolates. Recent studies have emphasized that molecular identification, genotypic diversity, biofilm production, and previous antifungal exposure significantly affect resistance patterns and therapeutic outcomes in HIV-associated oral candidiasis [55-57]. Therefore, future studies should include molecular identification methods, standardized resistance profiling, and more comprehensive clinical metadata to strengthen the interpretation of antifungal activity results.

Chitosan nanoparticles infused with cinnamaldehyde exhibit a pronounced antifungal efficacy, with MIC values in the microgram per milliliter (µg/mL) range. For instance, the antifungal potency of nanoencapsulated cinnamaldehyde in many experiments demonstrated a MIC of approximately 125 µg/mL (or 0.0125%) against *C. albicans*, suggesting that the nanoparticle formulation may surpass the efficacy of the unencapsulated chemical [13]. Besides that, the MIC values for fluconazole as an antifungal of *C. albicans* isolates from HIV patients generally range from 0.125 to over 64 µg/mL. As per the CLSI breakpoints, isolates with a MIC of ≤2 µg/mL are classified as susceptible, those with 4 µg/mL are deemed susceptible dose-dependent, and isolates with ≥8 µg/mL are categorized as resistant [6, 50]. Increased MICs signify diminished susceptibility and may be associated with clinical therapy failure. Therefore, MIC values for micafungin against *C. albicans* isolates are often low, frequently ≤0.03 µg/mL, indicating strong efficacy. CLSI breakpoints establish susceptibility as MIC ≤ 0.25 µg/mL. The low MIC values detected in clinical isolates from HIV patients indicate that micafungin is a dependable choice, particularly in instances of fluconazole resistance.

The clarification of MIC values in terms of cinnamaldehyde-equivalent concentration improves the interpretability and comparability of the present findings with previous antifungal studies and international susceptibility testing standards such as the CLSI and the European Committee on Antimicrobial Susceptibility Testing (EUCAST) [58, 59]. Since nanoformulations may vary substantially in encapsulation efficiency, particle composition, and active compound loading, reporting only percentage-based concentrations may not adequately reflect the actual antifungal dose delivered. Expressing MIC values in µg/mL

cinnamaldehyde equivalent therefore provides a more standardized basis for evaluating antifungal potency and comparing results across studies [60]. Future work should further standardize nanoformulation reporting by including encapsulation efficiency, loading capacity, particle stability, and release kinetics to facilitate reproducibility and clinical translation [61].

The observed variability in MIC values among *C. albicans* isolates (0.195–1.56%) may reflect differences in the biological and phenotypic characteristics of each isolate. Several mechanisms could contribute to this variation in antifungal susceptibility. One possible explanation is the presence of different resistance mechanisms among isolates, including alterations in cell membrane composition, increased efflux pump activity, biofilm-forming capacity, and stress-response adaptation [62, 63]. Isolates with higher MIC values may possess enhanced protective mechanisms that reduce intracellular accumulation of cinnamaldehyde or limit nanoparticle penetration. In contrast, isolates with lower MIC values may be more susceptible due to weaker membrane integrity or lower adaptive resistance capacity.

Additionally, genetic variability among clinical isolates obtained from HIV patients may influence their responsiveness to antifungal agents. Previous exposure to antifungal drugs such as azoles could also contribute to cross-tolerance phenomena, resulting in reduced susceptibility in some isolates [56]. Variations in cell wall thickness, ergosterol content, metabolic activity, and virulence-associated factors may further affect the interaction between cinnamaldehyde-chitosan nanocapsules and fungal cells [60]. The mucoadhesive and membrane-disruptive properties of chitosan, combined with the antifungal activity of cinnamaldehyde, may interact differently depending on the physiological state of each isolate. Therefore, the range of MIC values observed in this study likely reflects the heterogeneous nature of clinical *C. albicans* isolates. Future molecular and mechanistic studies are needed to identify the specific resistance pathways and cellular responses associated with varying susceptibility to cinnamaldehyde-based nanoformulations.

The present study has several limitations regarding experimental controls. Although RPMI 1640 medium was used as the growth control and blank chitosan nanoparticles were included as comparative controls, vehicle-only controls and direct head-to-head comparisons with free cinnamaldehyde and standard antifungal agents were not conducted. Previous studies have emphasized the importance of standardized experimental controls and comparative antifungal evaluations in nanoparticle-based antifungal research to ensure accurate interpretation of efficacy and specificity [27]. Future studies should therefore incorporate vehicle controls, free cinnamaldehyde, and reference antifungal drugs to better define the relative antifungal efficacy and specificity of the developed nanoformulation.

The spherical morphology and uniform size indicate successful nanoencapsulation formation, which is relevant for applications such as drug delivery or antibiofilm [63-65]. The scale bar in SEM images is often in the range of 1-5 microns to visually observe the aggregate or particle distribution. This provides an overview of the size distribution and surface texture of the particles that are very important in characterization [16]. The sample contains irregular, angular, and flaky particles, consistent with a crushed or fragmented material, possibly a mineral, polymer composite, or bio-based material. These nanoparticles demonstrate superior thermal stability, sustained or biphasic release characteristics, enhanced water solubility, and potent antimicrobial and antioxidant properties [66]. There is a mixture of flat surfaces, rough textures, and fine particulate flakes, indicating a heterogeneous material with potentially different phases or components.

Compared with conventional antifungal drugs such as fluconazole, cinnamaldehyde-chitosan nanocapsules may offer several potential advantages for the management of oral candidiasis. Fluconazole is widely used as a first-line antifungal therapy; however, prolonged use may lead to adverse effects, including hepatotoxicity, gastrointestinal disturbances, drug interactions, and the emergence of antifungal resistance, particularly among immunocompromised patients such as people living with HIV [67]. Recent studies have also highlighted the increasing prevalence of antifungal-resistant *C. albicans* species isolated from HIV-associated oral candidiasis, emphasizing the urgent need for alternative antifungal strategies [56].

In contrast, cinnamaldehyde is a natural bioactive compound with broad-spectrum antifungal and antibiofilm activity, while chitosan possesses intrinsic antimicrobial and mucoadhesive properties that may enhance localized drug retention and penetration at the site of infection [68, 69]. Nanoencapsulation may further improve the stability, solubility, controlled release profile, and bioavailability of cinnamaldehyde, potentially reducing the required therapeutic dose and minimizing systemic side effects. Previous in vitro studies have demonstrated enhanced antifungal efficacy of nano-cinnamaldehyde formulations against *C. albicans* biofilms compared with non-encapsulated formulations [70]. These characteristics may contribute to improved patient comfort and treatment compliance, especially for long-term or recurrent oral candidiasis therapy.

In addition to oral suspension formulations, the developed nanocapsules may also be adapted into various drug delivery systems, including oral gels, mucoadhesive films, mouth rinses, lozenges, and buccal sprays for localized antifungal therapy. Such delivery approaches could prolong contact time with oral mucosal tissues and improve therapeutic effectiveness. Recent studies have also explored cinnamaldehyde- and chitosan-based mucoadhesive films and nanoparticle systems for oral candidiasis management, supporting the feasibility of localized nanoformulation delivery [64-66].

Nevertheless, several challenges remain before clinical translation can be achieved. Large-scale production of nanocapsules requires optimization to ensure reproducibility, particle size uniformity, encapsulation efficiency, and long-term formulation stability during storage and distribution. Moreover, the cost of nanoformulation development and manufacturing may be higher than that of conventional antifungal formulations, potentially limiting accessibility in low-resource settings. Further studies evaluating formulation stability, cytotoxicity, pharmacokinetics, scalability, and in vivo therapeutic efficacy are therefore necessary to support future clinical application of cinnamaldehyde-chitosan nanocapsules as an alternative antifungal strategy for oral candidiasis [71-73].

This study has several limitations that should be considered. Because EDX analysis of polymeric nanoparticles is strongly influenced by sample coating and substrate artifacts, the present data were interpreted cautiously and were not used for

quantitative compositional analysis. The experimental design primarily focused on comparing free cinnamaldehyde and cinnamaldehyde-loaded chitosan nanoparticles to evaluate the effect of nanoencapsulation on antifungal activity; therefore, standard antifungal drugs such as fluconazole, nystatin, amphotericin B, or micafungin were not included as comparative positive controls. Consequently, the relative efficacy of the nanoformulation against clinically established antifungal therapies could not be determined.

In addition, the study involved a limited number of *C. albicans* clinical isolates (n = 8), which may restrict the generalizability of the findings. Another limitation of this study is the limited clinical characterization of the fungal isolates. Although all isolates were phenotypically identified as *C. albicans*, molecular identification and detailed antifungal resistance profiling were not conducted. In addition, information regarding prior antifungal exposure and the clinical history of the patients was incomplete. These factors may affect isolate susceptibility patterns and limit broader interpretation of the findings.

Cytotoxicity, biocompatibility, and formulation stability evaluations were also not performed, and the study was conducted exclusively under in vitro conditions without animal or clinical validation. Therefore, the safety, pharmacokinetics, mucosal retention, and therapeutic effectiveness of the formulation under physiological conditions remain unclear. Future studies should include larger isolate collections, standardized antifungal controls, cytotoxicity and stability analyses, as well as in vivo investigations to further validate the translational potential of the nanoformulation for oral antifungal applications.

Another limitation of this study is that the present study did not include a direct head-to-head comparison between cinnamaldehyde-loaded chitosan nanoparticles, free cinnamaldehyde, and standard antifungal drugs. Therefore, further studies are necessary to comprehensively evaluate the relative antifungal efficacy of the developed nanoformulation.

4. CONCLUSIONS

The cinnamaldehyde-loaded chitosan nanoencapsulation successfully produced nanoparticles with a mean particle size of 261.99 ± 21.06 nm, a PdI of 0.252, and a zeta potential of +19.34 ± 0.71 mV, indicating relatively uniform distribution, acceptable stability, and minimal aggregation. FTIR and UV–Vis analyses confirmed the successful incorporation of cinnamaldehyde within the chitosan matrix, while SEM and TEM observations revealed predominantly spherical nanoparticles with structural characteristics consistent with polymeric nanoencapsulation systems. EDX analysis was used only as a complementary method to support SEM observations, with Au signals attributed to the sputter-coating process.

The cinnamaldehyde-chitosan nanoparticles demonstrated promising in vitro antifungal activity against clinical *C. albicans* isolates associated with HIV-related oral candidiasis, although variations in MIC values indicated differences in isolate susceptibility. Despite these encouraging findings, the study was limited by the absence of comprehensive comparative controls and detailed isolate characterization. Therefore, further studies involving standardized antifungal comparisons, molecular resistance profiling, formulation optimization, release studies, cytotoxicity evaluation, and in vivo validation are necessary to strengthen the translational potential of this nanoformulation as an alternative antifungal therapy.

ACKNOWLEDGEMENTS

This research was funded by the Directorate of Research and Community Service, Directorate General of Research and Development, Ministry of Higher Education, Science, and Technology, under grant number No. 067/C3/DT/05.00/PL/2025. The funding body had no role in the design of the study, data collection, analysis, interpretation, or in writing the manuscript.

REFERENCES

[1] Erfaninejad, M., Zarei Mahmoudabadi, A., Maraghi, E., Hashemzadeh, M., Fatahinia, M. (2022). Epidemiology, prevalence, and associated factors of oral candidiasis in HIV patients from southwest Iran in post-highly active antiretroviral therapy era. Frontiers in Microbiology, 13: 983348. https://doi.org/10.3389/fmicb.2022.983348

[2] Ekwealor, C.C., Nweke, C.J., Anaukwu, C.G., Anakwenze, V.N., Ogbukagu, C.M., Mba, A.N. (2023). Prevalence and antifungal susceptibility pattern of oral candidiasis among HIV-infected patients in a Mission Hospital, southeast Nigeria. African Journal of Clinical & Experimental Microbiology, 24(3): 289-298. https://doi.org/10.4314/ajcem.v24i3.9

[3] Keyvanfar, A., Najafiarab, H., Talebian, N., Tafti, M.F., Adeli, G., Ghasemi, Z., Tehrani, S. (2024). Drug-resistant oral candidiasis in patients with HIV infection: A systematic review and meta-analysis. BMC Infectious Diseases, 24(1): 546. https://doi.org/10.1186/s12879-024-09442-6

[4] Azzaim, Y.A. (2023). Management of oral candidiasis in people living with HIV. Denta: Journal of Dentistry, 17(2): 75-83.

[5] Rachel, R., Anuradha, M., Leela, K.V. (2024). Evaluating the antifungal potential of cinnamaldehyde: A study of its efficacy against candida species. Journal of Pure & Applied Microbiology, 18(4): 2438-2445. https://doi.org/10.22207/JPAM.18.4.16

[6] Wang, X., Liu, B., Hayat, K., Xia, S., Cui, H., Yu, J. (2024). Fabrication and characterization of long-lasting antifungal film containing cinnamaldehyde-loaded complex coacervation microcapsules based on gelatin and gum Arabic. International Journal of Biological Macromolecules, 281: 136603. https://doi.org/10.1016/j.ijbiomac.2024.136603

[7] Saracino, I.M., Foschi, C., Pavoni, M., Spigarelli, R., Valerii, M.C., Spisni, E. (2022). Antifungal activity of natural compounds vs. candida spp.: A mixture of cinnamaldehyde and eugenol shows promising in vitro results. Antibiotics, 11(1): 73. https://doi.org/10.3390/antibiotics11010073

[8] Aniket, S., Ganesh, S., Kajal, P., Chandrashekhar, P., Sunil, M., Deepak, S. (2024). Phytochemical analysis and antifungal effect of extracted cinnamaldehyde against some fungal species. World, 20(3): 193-202. https://doi.org/10.30574/wjbphs.2024.20.3.1007

[9] Feng, J., Sun, L., Zhai, T., Liang, Q., Jiang, T., Chen, Z.

(2023). Preparation of cinnamaldehyde nanoemulsions: Formula optimization, antifungal activity, leaf adhesion, and safety assessment. Industrial Crops and Products, 200: 116825. https://doi.org/10.1016/j.indcrop.2023.116825
[10] Zhang, G., Li, T., Liu, J., Wu, X., Yi, H. (2023). Cinnamaldehyde-contained polymers and their biomedical applications. Polymers, 15(6): 1517. https://doi.org/10.3390/polym15061517
[11] Rizzo, S., Di Vito, M., Mazzinelli, E., Favuzzi, I., et al. (2023). Cinnamaldehyde loaded poly (lactide-co-glycolide) (PLGA) microparticles for antifungal delivery application against resistant Candida albicans and Candida glabrata. Plants, 12(13): 2437. https://doi.org/10.3390/plants12132437
[12] Mishra, P., Gupta, P., Pruthi, V. (2021). Cinnamaldehyde incorporated gellan/PVA electrospun nanofibers for eradicating Candida biofilm. Materials Science and Engineering: C, 119: 111450. https://doi.org/10.1016/j.msec.2020.111450
[13] Essid, R., Ayed, A., Djebali, K., Saad, H., et al. (2023). Anti-Candida and anti-leishmanial activities of encapsulated Cinnamomum verum essential oil in chitosan nanoparticles. Molecules, 28(15): 5681. https://doi.org/10.3390/molecules28155681
[14] Yu, W., You, H., Li, X., Wang, H., et al. (2024). pH-responsive chitosan hollow microspheres pro-flavor based on interfacial Schiff-base bonding for controlled release of cinnamaldehyde. Food Hydrocolloids, 156: 110260. https://doi.org/10.1016/j.foodhyd.2024.110260
[15] Barrera-Martínez, C.L., Meléndez-Ortiz, H.I., Padilla-Vaca, F., Atanase, L.I., Peralta-Rodríguez, R.D., Liakos, I. (2024). Dual loading of trans-cinnamaldehyde and either paclitaxel or curcumin in chitosan nanoparticles: Physicochemical characterization and biological evaluation against MDCK and HeLa cells. Polymers, 16(21): 3087. https://doi.org/10.3390/polym16213087
[16] Mondéjar-López, M., Castillo, R., Jiménez, A.J.L., Gómez-Gómez, L., Ahrazem, O., Niza, E. (2024). Polysaccharide film containing cinnamaldehyde-chitosan nanoparticles, a new eco-packaging material effective in meat preservation. Food Chemistry, 437: 137710. https://doi.org/10.1016/j.foodchem.2023.137710
[17] Saeedi, M., Vahidi, O., Moghbeli, M.R., Ahmadi, S., et al. (2022). Customizing nano-chitosan for sustainable drug delivery. Journal of Controlled Release, 350: 175-192. https://doi.org/10.1016/j.jconrel.2022.07.038
[18] Sangnim, T., Dheer, D., Jangra, N., Huanbutta, K., Puri, V., Sharma, A. (2023). Chitosan in oral drug delivery formulations: A review. Pharmaceutics, 15(9): 2361. https://doi.org/10.3390/pharmaceutics15092361
[19] Hosseini, S.F., Ghaderi, J., Gómez-Guillén, M.C. (2022). Tailoring physico-mechanical and antimicrobial/antioxidant properties of biopolymeric films by cinnamaldehyde-loaded chitosan nanoparticles and their application in packaging of fresh rainbow trout fillets. Food Hydrocolloids, 124: 107249. https://doi.org/10.1016/j.foodhyd.2021.107249
[20] Cheng, C.H., Tu, Y.Y., Lin, J.C. (2022). Studies of mercaptosuccinic acid-crosslinked chitosan hydrogel with grafted cinnamaldehyde and silver nanoparticles for antibacterial biomedical application. International Journal of Molecular Sciences, 23(23): 14806. https://doi.org/10.3390/ijms232314806
[21] Harugade, A., Sherje, A.P., Pethe, A. (2023). Chitosan: A review on properties, biological activities and recent progress in biomedical applications. Reactive and Functional Polymers, 191: 105634. https://doi.org/10.1016/j.reactfunctpolym.2023.105634
[22] Ul-Islam, M., Alabbosh, K.F., Manan, S., Khan, S., Ahmad, F., Ullah, M.W. (2024). Chitosan-based nanostructured biomaterials: Synthesis, properties, and biomedical applications. Advanced Industrial and Engineering Polymer Research, 7(1): 79-99. https://doi.org/10.1016/j.aiepr.2023.07.002
[23] Algharib, S.A., Dawood, A., Zhou, K., Chen, D., et al. (2022). Preparation of chitosan nanoparticles by ionotropic gelation technique: Effects of formulation parameters and in vitro characterization. Journal of Molecular Structure, 1252: 132129. https://doi.org/10.1016/j.molstruc.2021.132129
[24] Shehabeldine, A.M., Salem, S.S., Ali, O.M., Abd-Elsalam, K.A., Elkady, F.M., Hashem, A.H. (2022). Multifunctional silver nanoparticles based on chitosan: Antibacterial, antibiofilm, antifungal, antioxidant, and wound-healing activities. Journal of Fungi, 8(6): 612. https://doi.org/10.3390/jof8060612
[25] Yang, K., Liu, A., Hu, A., Li, J., et al. (2021). Preparation and characterization of cinnamon essential oil nanocapsules and comparison of volatile components and antibacterial ability of cinnamon essential oil before and after encapsulation. Food Control, 123: 107783. https://doi.org/10.1016/j.foodcont.2020.107783
[26] Utami, T.M., Wulandari, W.T., Tuslinah, L. (2022). Characteristics of curcumin nanoparticles with the addition of eudragit using the ionic gelation method. In Proceedings of the National Seminar on Dissemination of Research Results of the Undergraduate Pharmacy Study Program.
[27] Poznanski, P., Hameed, A., Orczyk, W. (2023). Chitosan and chitosan nanoparticles: Parameters enhancing antifungal activity. Molecules, 28(7): 2996. https://doi.org/10.3390/molecules28072996
[28] Jayathilaka, E.T., Nikapitiya, C., De Zoysa, M., Whang, I. (2022). Antimicrobial peptide octominin-encapsulated chitosan nanoparticles enhanced antifungal and antibacterial activities. International Journal of Molecular Sciences, 23(24): 15882. https://doi.org/10.3390/ijms232415882
[29] Nandiyanto, A.B.D., Ragadhita, R., Fiandini, M. (2023). Interpretation of Fourier transform infrared spectra (FTIR): A practical approach in the polymer/plastic thermal decomposition. Indonesian Journal of Science and Technology, 8(1): 113-126. https://ijost.upi.edu/index.php/ijost/article/view/365.
[30] Lasalvia, M., Capozzi, V., Perna, G. (2021). Discrimination of different breast cell lines on glass substrate by means of Fourier transform infrared spectroscopy. Sensors, 21(21): 6992. https://doi.org/10.3390/s21216992
[31] Gao, X., Liu, N., Wang, Z., Gao, J., et al. (2021). Development and optimization of chitosan nanoparticle-based intranasal vaccine carrier. Molecules, 27(1): 204. https://doi.org/10.3390/molecules27010204
[32] Hossain, M.S., Ahmed, S. (2023). FTIR spectrum analysis to predict the crystalline and amorphous phases of hydroxyapatite: A comparison of vibrational motion

to reflection. RSC Advances, 13(21): 14625-14630. https://doi.org/10.1039/d3ra02580b
[33] Jakhmola, A., Onesto, V., Gentile, F., Kashkooli, F.M., et al. (2024). Polyvinyl alcohol assisted citrate based reduction of gold (III) ions: Theoretical design and experimental study on green synthesis of spherical and biocompatible gold nanoparticles. Materials Today Sustainability, 28: 101012. https://doi.org/10.1016/j.mtsust.2024.101012
[34] Filippov, S.K., Khusnutdinov, R., Murmiliuk, A., Inam, W., Zakharova, L.Y., Zhang, H., Khutoryanskiy, V.V. (2023). Dynamic light scattering and transmission electron microscopy in drug delivery: A roadmap for correct characterization of nanoparticles and interpretation of results. Materials Horizons, 10(12): 5354-5370. https://doi.org/10.1039/d3mh00717k
[35] Carlton, C.E., Zorro, F., Caturla, M.J., Aoki, T., Zhu, Y., Amodeo, J., Ferreira, P.J. (2025). Nanocompression of 20 nm Silver Nanoparticles: In situ Aberration-Corrected TEM and Atomistic Simulations. Small, 21(4): 2405292. https://doi.org/10.1002/smll.202405292
[36] Ramadhan, S.A., Ali, D.S. (2025). Innovations in core–shell nanoparticles: Advancing drug delivery solutions and precision medicine. OMICS: A Journal of Integrative Biology, 29(3): 73-86. https://doi.org/10.1089/omi.2024.0182
[37] Guo, L., Zhao, Q., Wang, M. (2024). Core–shell microspheres with encapsulated gold nanoparticle carriers for controlled release of anti-cancer drugs. Journal of Functional Biomaterials, 15(10): 277. https://doi.org/10.3390/jfb15100277
[38] Negi, A., Kesari, K.K. (2022). Chitosan nanoparticle encapsulation of antibacterial essential oils. Micromachines, 13(8): 1265. https://doi.org/10.3390/mi13081265
[39] Yousefi, S., Ghasemi, B., Nikolova, M.P. (2022). Morpho/Opto-structural characterizations and XRD-assisted estimation of crystallite size and strain in MgO nanoparticles by applying Williamson–Hall and size–strain techniques. Journal of Cluster Science, 33(5): 2197-2207. https://doi.org/10.1007/s10876-021-02144-y
[40] Quevedo, A.C., Guggenheim, E., Briffa, S.M., Adams, J., et al. (2021). UV-Vis spectroscopic characterization of nanomaterials in aqueous media. Journal of Visualized Experiments, 176: e61764. https://doi.org/10.3791/61764
[41] Cinar, K., Parasiz, S.A., Akbulut, M., Eruslu, S.O. (2022). An experimental and numerical investigation of particle morphology effect on the elasto-plastic behavior of particle-filled composites. Fibers and Polymers, 23(9): 2694-2711. https://doi.org/10.1007/s12221-022-4382-y
[42] Wang, G., Huang, Y. (2023). Numerical investigation on the fracture-bridging behaviors of irregular non-spherical stiff particulate lost circulation materials in a fractured leakage well section. Geoenergy Science and Engineering, 223: 211577. https://doi.org/10.1016/j.geoen.2023.211577
[43] Liang, F., Liu, C., Geng, J., Chen, N., Lai, W., Mo, H., Liu, K. (2024). Chitosan–fucoidan encapsulating cinnamaldehyde composite coating films: Preparation, pH-responsive release, antibacterial activity and preservation for litchi. Carbohydrate Polymers, 333: 121968. https://doi.org/10.1016/j.carbpol.2024.121968
[44] Prananda, A.T., Prayugo, B., Dewi, F., Syahputra, R.A., et al. (2024). Unveiling the functional food properties of Pepromia pellucida: Phytochemical profiling, antioxidative potential, and their nanoemulsion fraction in wound healing efficacy. Journal of Agriculture and Food Research, 16: 101156. https://doi.org/10.1016/j.jafr.2024.101156
[45] Gutiérrez-Ruíz, S.C., Cortes, H., González-Torres, M., Almarhoon, Z.M., Gürer, E.S., Sharifi-Rad, J., Leyva-Gómez, G. (2024). Optimize the parameters for the synthesis by the ionic gelation technique, purification, and freeze-drying of chitosan-sodium tripolyphosphate nanoparticles for biomedical purposes. Journal of Biological Engineering, 18(1): 12. https://doi.org/10.1186/s13036-024-00403-w
[46] Butreddy, P., Heo, J., Rampal, N., Liu, T., et al. (2024). Ion correlations decrease particle aggregation rate by increasing hydration forces at interfaces. ACS Nano, 18(38): 26047-26055. https://doi.org/10.1021/acsnano.4c05563
[47] Chen, Y., Yu, Z., Zhu, G., Xu, H., Lin, N. (2024). High-throughput molecular dynamics study and turbidity analysis on clustering and agglomeration of cellulose nanocrystals in suspensions. Langmuir, 41(1): 1013-1023. https://doi.org/10.1021/acs.langmuir.4c04310
[48] Clares, A.P., Gao, Y., Stebbins, R., van Duin, A.C., Manogharan, G. (2022). Increasing density and mechanical performance of binder jetting processing through bimodal particle size distribution. Materials Science in Additive Manufacturing, 1(3): 20. https://doi.org/10.18063/msam.v1i3.20
[49] Faturachman, G.F., Ramanda, A.A., Maharani, S., Latif, L.A., Belo, G.A.G., Al Ayubi, S.G. (2025). Application of Fourier transform infrared spectroscopy (FTIR) for quantitative analysis of pharmaceutical compounds. Indonesian Journal of Pharmaceutical Education, 5(1): 27-33. https://doi.org/10.37311/ijpe.v5i1.23309
[50] Sultan, M., Youssef, A.M., Taha, G. (2024). Potential antimicrobial cotton fabrics treated with cinnamaldehyde/chitosan-alginate nanocapsules for food packaging purposes. International Journal of Biological Macromolecules, 279: 135384. https://doi.org/10.1016/j.ijbiomac.2024.135384
[51] Upadhyay, A., Ullas, A.V. (2023). Compressive strength and modulus of poly (dimethylsiloxane)-hollow glass microballoons syntactic foams reinforced with nanoclay. Materials Today: Proceedings, 80: 846-850. https://doi.org/10.1016/j.matpr.2022.11.318
[52] Fu, Y.P., Yang, H., Liu, H. L., Li, Y.H., Chen, X.L., Cui, H.L., Wang, J.J. (2024). Synthesis, structure, fluorescence and photocatalytic properties of two complexes based on a dimethylimidazole biphenyl/isophthalic acid ligand. Journal of Molecular Structure, 1305: 137741. https://doi.org/10.1016/j.molstruc.2024.137741
[53] Aldakheel, R.K., Gondal, M.A., Almessiere, M.A., Rehman, S., Nasr, M.M., Alsalem, Z., Khan, F.A. (2021). Spectrochemical analysis using LIBS and ICP-OES techniques of herbal medicine (Tinnevelly Senna leaves) and its anti-cancerous/antibacterial applications. Arabian Journal of Chemistry, 14(12): 103451. https://doi.org/10.1016/j.arabjc.2021.103451
[54] Lawal, U., Kumar, N., Samyuktha, R., Gopi, A., et al. (2024). Poly (lactic acid)/amine grafted mesoporous silica-based composite for food packaging application.

International Journal of Biological Macromolecules, 277: 134567. https://doi.org/10.1016/j.ijbiomac.2024.134567

[55] Alves, A.M.C.V., de Brito, É.H.S., de Araújo, M.F.M., de Hollanda Celestino, J.J., et al. (2024). Antifungal susceptibility and Candida sp. biofilm production in clinical isolates of HIV-positive brazilian patients under Haart therapy. Biomedicines, 12(2): 310. https://doi.org/10.3390/biomedicines12020310

[56] Erfaninejad, M., Mahmoudabadi, A.Z., Hashemzadeh, M., Maraghi, E., Fatahinia, M. (2024). Characteristics of Candida albicans derived from HIV-positive individuals with oral candidiasis: Genotyping, phenotypic variation, antifungal susceptibility, and biofilm formation. Journal of Clinical Laboratory Analysis, 38(19-20): e25103. https://doi.org/10.1002/jcla.25103

[57] Hui, S.T., Gifford, H., Rhodes, J. (2024). Emerging antifungal resistance in fungal pathogens. Current Clinical Microbiology Reports, 11(2): 43-50. https://doi.org/10.1007/s40588-024-00219-8

[58] Clinical and Laboratory Standards Institute (CLSI). (2022). Reference Method for Broth Dilution Antifungal Susceptibility Testing of Yeasts (CLSI standard M27, 5th ed.). CLSI.

[59] Simões, E.A. (2022). Respiratory syncytial virus disease in young children and older adults in Europe: A burden and economic perspective. The Journal of Infectious Diseases, 226(Supplement_1): S1-S9. https://doi.org/10.1093/infdis/jiac252

[60] Atala, C., Reyes, S.A., Molina-Montenegro, M.A. (2023). Assessing the importance of native mycorrhizal fungi to improve tree establishment after wildfires. Journal of Fungi, 9(4): 421. https://doi.org/10.3390/jof9040421

[61] Qiao, Z., Wei, X., Liu, H., Liu, K., Gao, C. (2023). Seed-mediated synthesis of thin gold nanoplates with tunable edge lengths and optical properties. Nanomaterials, 13(4): 711. https://doi.org/10.3390/nano13040711

[62] Pappas, P.G., Lionakis, M.S., Arendrup, M.C., Ostrosky-Zeichner, L., Kullberg, B.J. (2018). Invasive candidiasis. Nature Reviews Disease Primers, 4(1): 18026. https://doi.org/10.1097/md.0000000000015933

[63] Van Leeuwen, P.T., Brul, S., Zhang, J., Wortel, M.T. (2023). Synthetic microbial communities (SynComs) of the human gut: Design, assembly, and applications. FEMS Microbiology Reviews, 47(2): fuad012. https://doi.org/10.1093/femsre/fuad012

[64] Mu, R., Zhang, H., Zhang, Z., Li, X., Ji, J., Wang, X., Gu, Y., Qin, X. (2023). Trans-cinnamaldehyde loaded chitosan based nanocapsules display antibacterial and antibiofilm effects against cavity-causing Streptococcus mutans. Journal of Oral Microbiology, 15(1): 2243067. https://doi.org/10.1080/20002297.2023.2243067

[65] Tavassoli, M., Khezerlou, A., Sani, M.A., Hashemi, M., et al. (2024). Methylcellulose/chitosan nanofiber-based composites doped with lactoferrin-loaded Ag-MOF nanoparticles for the preservation of fresh apple. International Journal of Biological Macromolecules, 259: 129182. https://doi.org/10.1016/j.ijbiomac.2023.129182

[66] National Institutes of Health. (2024). Guidelines for the prevention and treatment of opportunistic infections in adults and adolescents with HIV: Candidiasis (mucocutaneous). https://clinicalinfo.hiv.gov/en/guidelines/hiv-clinical-guidelines-adult-and-adolescent-opportunistic-infections/candidiasis-0.

[67] Cunha, A.L.A., Alcântara, A.A., Viana, Y.N., De Aguiar, F.L.L., dos Santos Fontenelle, R.O., Barbosa, F.C.B. (2026). Antifungal potential of trans-cinnamaldehyde: A review. Archives of Current Research International, 26(1): 137-148. https://doi.org/10.9734/acri/2026/v26i11709

[68] Abiraami, N.S., Arvind, M. (2024). Effectiveness chitosan nanoparticle as an antifungal agent in Management of oral candidiasis-a systematic. Korean Journal of Physiology and Pharmacology, 28(2): 362-370. https://doi.org/10.25463/kjpp.28.2.2024.4

[69] Molania, T., Saeedi, M., Morteza-Semnani, K., Negarandeh, R., et al. (2025). Antifungal efficacy of cinnamaldehyde and nano-cinnamaldehyde particles against candidiasis: An in-vitro study. BMC Oral Health, 25(1): 1432. https://doi.org/10.1186/s12903-025-06804-7

[70] Akhriani, A.A., Mutmainnah, S.F., Musyrifah, N., Arfansyah, A., et al. (2026). Formulation of mucoadhesive dissolving film containing cinnamaldehyde and chitosan incorporating papain enzyme for inhibit oral candidiasis: In vitro study. Scientific Reports, 16: 16715. https://doi.org/10.1038/s41598-026-45154-4

[71] NS, S.A., Pillai, D.S., Shanmugam, R. (2024). The antifungal activity of chitosan nanoparticle-incorporated probiotics against oral candidiasis. Cureus, 16(9): e70093. https://doi.org/10.7759/cureus.70093

[72] Shakib, P., Fallahi, S., Goudarzi, G., Somaghian, S.A., Amiri, S., Delfan, S.N., Cheraghipour, K. (2025). Antifungal activity of chitosan nanocomposites against Candida albicans: A systematic review. Current Bioactive Compounds, 21(2): E160424228952. https://doi.org/10.2174/0115734072297928240404074703

[73] Anuța, V., Talianu, M.T., Dinu-Pîrvu, C.E., Ghica, M.V., Prisada, R.M., Albu Kaya, M.G., Popa, L. (2022). Molecular mapping of antifungal mechanisms accessing biomaterials and new agents to target oral candidiasis. International Journal of Molecular Sciences, 23(14): 7520. https://doi.org/10.3390/ijms23147520